Delayed Southern Hemisphere Climate Change Induced by Stratospheric Ozone Recovery, as Projected by the CMIP5 Models

ELIZABETH A. BARNES

Lamont-Doherty Earth Observatory, Columbia University, Palisades, New York

NICHOLAS W. BARNES

Department of Computer Science and Engineering, University of Minnesota, Twin Cities, Minneapolis, Minnesota

LORENZO M. POLVANI

Lamont-Doherty Earth Observatory, Columbia University, Palisades, and Department of Applied Physics and Applied Math, Columbia University, New York, New York

(Manuscript received 20 April 2013, in final form 5 August 2013)

ABSTRACT

Stratospheric ozone is expected to recover by the end of this century because of the regulation of ozone-depleting substances by the Montreal Protocol. Targeted modeling studies have suggested that the climate response to ozone recovery will greatly oppose the climate response to rising greenhouse gas (GHG) emissions. However, the extent of this cancellation remains unclear since only a few such studies are available. Here, a much larger set of simulations performed for phase 5 of the Coupled Model Intercomparison Project is analyzed, which includes ozone recovery. It is shown that the closing of the ozone hole will cause a delay in summertime [December–February (DJF)] Southern Hemisphere climate change between now and 2045. Specifically, it is found that the position of the jet stream, the width of the subtropical dry zones, the seasonality of surface temperatures, and sea ice concentrations all exhibit significantly reduced summertime trends over the first half of the twenty-first century as a consequence of ozone recovery. After 2045, forcing from GHG emissions begins to dominate the climate response. Finally, comparing the relative influences of future GHG emissions and historic ozone depletion, it is found that the simulated DJF tropospheric circulation changes between 1965 and 2005 (driven primarily by ozone depletion) are larger than the projected changes in any future scenario over the entire twenty-first century.

1. Introduction

Polar stratospheric ozone depletion has induced changes in the Southern Hemisphere climate with observational evidence of its impact on the atmospheric [Roscoe and Haigh (2007); Lee and Feldstein (2013); see Thompson et al. (2011) for a recent review], oceanic (Waugh et al. 2013), and hydrological (Kang et al. 2011) circulations. Modeling-based studies have documented the impact of the Montreal Protocol in mitigating future sea ice loss (Smith et al. 2012) and changes in Earth's hydroclimate (Wu et al. 2012) that would have occurred with unabated stratospheric ozone depletion. Looking to the future, the effects of stratospheric ozone recovery on Southern Hemisphere climate are expected to counteract the effects of greenhouse gas warming (e.g., Arblaster et al. 2011; Polvani et al. 2011a; McLandress et al. 2011; Wilcox et al. 2012).

Previous studies have focused on targeted, ozone-on–ozone-off simulations to determine the importance of past and future stratospheric ozone changes on the climate system (e.g., Sigmond and Fyfe 2010; Polvani et al. 2011b; Smith et al. 2012; Wu et al. 2012). While these single-forcing model experiments are clean and unambiguous tools to determine the influence of ozone recovery on global climate, they inherently exclude feedbacks between the transient greenhouse gas–induced response and the response resulting from ozone recovery. Additional studies (e.g., McLandress et al. 2011; Polvani et al.

Corresponding author address: Elizabeth A. Barnes, Department of Atmospheric Science, Colorado State University, 1371 Campus Delivery, Fort Collins, CO 80523-1371.
E-mail: eabarnes@atmos.colostate.edu

DOI: 10.1175/JCLI-D-13-00246.1

2011a) analyze output from a single coupled general circulation model that is forced with both greenhouse gases (GHGs) and stratospheric ozone depletion and recovery and thus are able to quantify the relative importance of stratospheric ozone recovery on future climate trends.

The climate models run for the Coupled Model Intercomparison Projects (CMIP) offer an important, additional dataset to explore the role of ozone recovery over the coming century in a large multimodel ensemble. As is now well documented (Cordero and Forster 2006; Son et al. 2008), only a subset of the models run for the phase 3 of CMIP (CMIP3) included time-varying stratospheric ozone (other than the seasonal cycle), and for those that did, no consistent ozone depletion and recovery time series was used. In contrast, in the most recent phase 5 of CMIP (CMIP5) all models included time-varying ozone fields, using a broad range of methods [e.g., coupled chemistry climate models, semioffline calculations, prescribed depletion, and recovery; see Eyring et al. (2013) for details]. In addition, a large number of CMIP5 models included a well-resolved stratosphere (high top), potentially allowing for a better representation of the atmospheric response to polar stratospheric ozone changes (Wilcox et al. 2012). The CMIP5 models, therefore, provide an unprecedented multimodel ensemble to assess the role of ozone recovery on the transient twenty-first-century Southern Hemisphere climate.

Since time-varying ozone is included in all of the CMIP5 simulations, one cannot follow the CMIP3 approach—where models were separated into those with and without varying stratospheric ozone—to bring out the effect of ozone changes (e.g., Son et al. 2008, 2009). Instead, we use a different technique: taking advantage of the fact that stratospheric ozone began to decline in the 1970s, reached a minimum around 2005, and is expected to largely recover by midcentury (Eyring et al. 2013), we define four time periods over which the ozone forcing has very different trends (e.g., preozone depletion, ozone depletion, ozone recovery, and postozone recovery). We also exploit the seasonal cycle of the ozone forcing (Thompson and Solomon 2002; Eyring et al. 2013): the cooling of the stratosphere associated with springtime stratospheric ozone depletion induces the largest changes in tropospheric circulation in austral summer [December–February (DJF)], where the lagged response is because of the time it takes for the stratospheric signal to reach the lower troposphere (Thompson and Solomon 2002; Polvani et al. 2011b). As in Polvani and Solomon (2012), we exploit the seasonal dependence of the stratospheric ozone forcing to distinguish it from the response to greenhouse gas forcing (which does not have a seasonal cycle), highlighting the distinct signature of ozone recovery on the Southern Hemisphere climate system.

In a nutshell, we demonstrate that the CMIP5 models project a significant delay in summertime Southern Hemisphere climate change between 2005 and 2045 resulting from ozone recovery largely canceling the effects of other forcings. The effects of ozone recovery are found in the winds, the hydrological cycle, the near-surface air temperatures, and the sea ice concentrations. We will additionally show that circulation changes resulting from ozone depletion between 1965 and 2005 are larger than the changes in any scenario over the entire twenty-first century.

2. Data and methods

a. CMIP5 climate models and scenarios

We use model output from the CMIP5 archive. Specifically, we analyze the monthly-mean, zonal-mean zonal wind, 2-m air temperature, sea ice concentration, precipitation, and evaporation from four forcing scenarios: historical (1900–2005) and representative concentration pathways (RCPs) RCP2.6, RCP4.5, and RCP8.5 (2006–99). The RCP2.6, RCP4.5, and RCP8.5 scenarios correspond to futures with varying levels of anthropogenic emissions. RCP2.6 is an aggressive mitigation scenario, where emissions of GHG and the total radiative forcing at the top of the atmosphere stops increasing near 2050 with a maximum value of $3.0\,\mathrm{W\,m^{-2}}$ and declines to $2.6\,\mathrm{W\,m^{-2}}$ by 2100. RCP4.5 is a stabilization scenario, where emissions of GHG are constant after 2150; however, emission increases (and the total radiative forcing) level off substantially after 2075 [emissions of CO_2 increase at only 40% of their 2005–50 rate; see Table 4 of Meinshausen et al. (2011)] and the radiative forcing reaches $4.5\,\mathrm{W\,m^{-2}}$ by 2100. RCP8.5 is the transient scenario with the largest radiative forcing of $8.5\,\mathrm{W\,m^{-2}}$ by 2100 that continues to increase thereafter. Additional details about each scenario can be found in Meinshausen et al. (2011).

We analyze the three RCPs, rather than just one 1) to quantify the relative importance of stratospheric ozone recovery across a range of possible futures and 2) to exploit the fact that since the magnitude and timing of stratospheric ozone changes are similar across all of the RCPs, any difference in the climate responses can be directly attributed to forcings other than ozone. Conversely, trends that are found to be very similar across all RCPs are likely the fingerprint of stratospheric ozone. Therefore, exploration of the different RCPs allows us to bring out the ozone recovery signal.

TABLE 1. Data availability of CMIP5 model output.

Model name	Model expansion	Zonal wind	2-m temperature, sea ice, precipitation, and evaporation
BCC-CSM1.1	Beijing Climate Center, Climate System Model, version 1.1	x	x
CanESM2	Second Generation Canadian Earth System Model	x	x
CSIRO-Mk3.6.0	Commonwealth Scientific and Industrial Research Organisation Mark, version 3.6.0	x	x
GFDL-CM3	Geophysical Fluid Dynamics Laboratory Climate Model, version 3	x	x
GFDL-ESM2G	Geophysical Fluid Dynamics Laboratory Earth System Model coupled with Generalized Ocean Layer Dynamics (GOLD) component (ESM2G)	x	x
GFDL-ESM2M	Geophysical Fluid Dynamics Laboratory Earth System Model coupled with Modular Ocean Model, version 4 (MOM4), component (ESM2M)	x	x
GISS-E2-H	Goddard Institute for Space Studies Model E2, coupled with the Hybrid Coordinate Ocean Model (HYCOM)	x	
GISS-E2-R	Goddard Institute for Space Studies Model E2, coupled with the Russell ocean model	x	x
HadGEM2-ES	Hadley Centre Global Environment Model, version 2, Earth System	x	x
IPSL-CM5A-LR	L'Institut Pierre-Simon Laplace Coupled Model, version 5A, coupled with the Nucleus for European Modelling of the Ocean (NEMO), low resolution	x	x
IPSL-CM5A-MR	L'Institut Pierre-Simon Laplace Coupled Model, version 5A, coupled with NEMO, mid resolution	x	x
MIROC5	Model for Interdisciplinary Research on Climate, version 5	x	x
MIROC-ESM	Model for Interdisciplinary Research on Climate, Earth System Model	x	x
MIROC-ESM-CHEM	Model for Interdisciplinary Research on Climate, Earth System Model, Chemistry Coupled	x	x
MPI-ESM-LR	Max Planck Institute Earth System Model, low resolution	x	x
MPI-ESM-MR	Max Planck Institute Earth System Model, medium resolution	x	
MRI-CGCM3	Meteorological Research Institute Coupled Atmosphere–Ocean General Circulation Model, version 3	x	x
NorESM1-M	Norwegian Earth System Model, version 1 (mid resolution)	x	x

For the sake of brevity, we analyze one ensemble member from every model that provided monthly-mean data for all four scenarios (18 models for zonal wind and 16 models for the other variables; see Table 1). Although all of the CMIP5 models included some form of stratospheric ozone depletion and recovery, some modeling groups prescribed ozone following the International Global Atmospheric Chemistry Project (IGAC)/Stratospheric Processes and Their Role in Climate (SPARC) ozone database (Cionni et al. 2011), while others employed interactive chemistry that calculates stratospheric ozone online or semioffline [see Eyring et al. (2013) for additional details]. Here, we are interested in whether a robust signal from ozone recovery is evident in the projections of Southern Hemisphere climate, and thus we consider all of the models regardless of their stratospheric ozone scheme.

TABLE 2. Data availability of CMIP3 model output, distinguishing those models with fixed stratospheric ozone and those that include time-varying (seasonal) stratospheric ozone.

Ozone data	Model name	Model expansion
Fixed ozone		
	BCCR-BCM2.0	Bjerknes Centre for Climate Research Bergen Climate Model, version 2.0
	CGCM3.1 (T63)	Canadian Centre for Climate Modelling and Analysis (CCCma) Coupled Global Climate Model, version 3.1 (spectral T63 resolution)
	GISS-AOM	Goddard Institute for Space Studies, Atmosphere–Ocean Model
	FGOALS-g1.0	Flexible Global Ocean–Atmosphere–Land System Model gridpoint, version 1.0
	INM-CM3.0	Institute of Numerical Mathematics Coupled Model, version 3.0
	IPSL-CM4	L'Institut Pierre-Simon Laplace Coupled Model, version 4
	MRI-CGCM2.3.2	Meteorological Research Institute Coupled Atmosphere–Ocean General Circulation Model, version 2.3.2a
Varying ozone		
	ECHAM5/MPI-OM	ECHAM5/Max Planck Institute Ocean Model
	CCSM3	Community Climate System Model, version 3
	CSIRO-Mk3.0	Commonwealth Scientific and Industrial Research Organisation Mark, version 3.0
	GFDL-CM2.0	Geophysical Fluid Dynamics Laboratory Climate Model, version 2.0
	GFDL-CM2.1	Geophysical Fluid Dynamics Laboratory Climate Model, version 2.1
	GISS-EH	Goddard Institute for Space Studies Model E-H
	GISS-ER	Goddard Institute for Space Studies Model E-R
	INGV-SXG	Istituto Nazionale di Geofisica e Vulcanologia, SINTEX-G
	PCM	Parallel Climate Model
	UKMO-HadCM3	Met Office Hadley Centre Coupled Model, version 3
	UKMO-HadGEM1	Met Office Hadley Centre Global Environment Model, version 1

b. CMIP3 climate models

We also compare the CMIP5 results with those from the twentieth-century climate (20C3M; present day) and A1B (future warming) model integrations from CMIP3 (Meehl et al. 2007). Those models are separated into two categories, those with time-varying ozone in both the 20C3M and A1B simulations (varyO3; 11 models) and those with fixed ozone (other than the seasonal cycle) in both simulations (fixO3; 7 models) (see Table 2). Our categories are identical to those in Son et al. (2010), except that we have omitted Centre National de Recherches Météorologiques Coupled Global Climate Model, version 3 (CNRM-CM3), because of some confusion as to whether time-varying ozone was or was not included [see discussion in Son et al. (2010)].

c. Choice of time periods

To bring out the ozone signal, all time series are divided into four time periods: 1) historical (HIST; 1900–70), 2) ozone depletion (O3DEPL; 1970–2005), 3) ozone recovery (O3RCVR; 2005–45), and 4) the end of the twenty-first century (FUTR; 2045–99) when ozone has largely recovered and GHG emissions dominate the climate forcing. These four periods naturally emerge from the data analysis (as will be described), but their definitions are also supported by considering the evolution of October stratospheric ozone over the Southern Hemisphere polar cap (see Eyring et al. 2013, their Fig. 6f): stratospheric ozone begins to decline in the 1970s, reaches a minimum at 2005, and recovers to its 1980 level by 2040–45 in the IGAC/SPARC ozone database and in models with interactive chemistry. It should be clear that the qualitative results of this study are not sensitive to the exact definition of the four periods.

d. Analysis methods

In the following analysis, the jet position is defined, for each month, as the latitude of maximum 700–850-hPa zonal-mean zonal wind, following the method of Barnes and Polvani (2013). For the multimodel mean fields, data from each model simulation is interpolated to a 2° by 2° latitude–longitude grid before plotting. The meridional extent of the dry zone is defined, for each month, as the latitude of the zero crossing between 30° and 60°S of the zonal-mean precipitation minus evaporation

profile. For both the jet position and the dry zone edge, the zonal-mean model data are interpolated using a cubic spline to a 0.1° grid before the final calculation.

Plotted time series are smoothed using a 10-yr moving average filter with time step of 1 yr. We have performed similar analysis with unsmoothed data, and the smoothing is not essential to the conclusions of this study. The best-fit slopes of the time series are calculated from the individual smoothed model data using linear least squares regression, and the bounds on the slopes denote the symmetric 95% confidence interval. Note that the 10-yr smoothing causes the O3DEPL period (1970–2005) to include data from 2006 to 2010, when the different RCPs begin to diverge. Thus, trends during the O3DEPL period differ slightly depending on the RCP used in the smoothing.

3. Seasonal shifts of the circulation

The position of the Southern Hemisphere midlatitude jet stream determines the path of storms and drives ocean circulations and sea ice dispersion, and stratospheric ozone depletion is known to cause a poleward shift of the Southern Hemisphere jet in summer. As for previous generations of climate models (Kidston and Gerber 2010), the CMIP5 models exhibit an up to 8° equatorward bias of the Southern Hemisphere jet stream position (Barnes and Polvani 2013; Ceppi et al. 2012). Thus, we define for each model simulation the ''relative jet position'' as the latitude of the jet with respect to its average 1900–10 latitude. By plotting the relative position of the jet (shift) over time between 1900 and 2100 in each model, and then averaging the results together in Fig. 1, we avoid the difficulty of model spread masking the coherent poleward jet shift.

Four distinct time periods naturally emerge from the time series of jet position in Fig. 1 (which represents the multimodel mean): 1) HIST (1900–70), 2) O3DEPL (1970–2005), 3) O3RCVR (2005–45), and 4) GHG-dominated FUTR (2045–99). Throughout the HIST period, the jet position remains relatively unchanged, but a sharp southward shift is evident during the O3DEPL period, with the multimodel mean showing a −1.78° shift of the jet in DJF in RCP8.5 (see Table 3): this number is in excellent agreement with previous studies (see Table 2 of Polvani et al. 2011b).

If the large poleward shift of the jet during O3DEPL was primarily a result of GHG emissions (which are increasing over this period for all scenarios), then one would expect the poleward trend in the jet position to continue into the twenty-first century. Instead, the trend in jet position halts abruptly around 2005, providing strong evidence that ozone recovery is canceling the

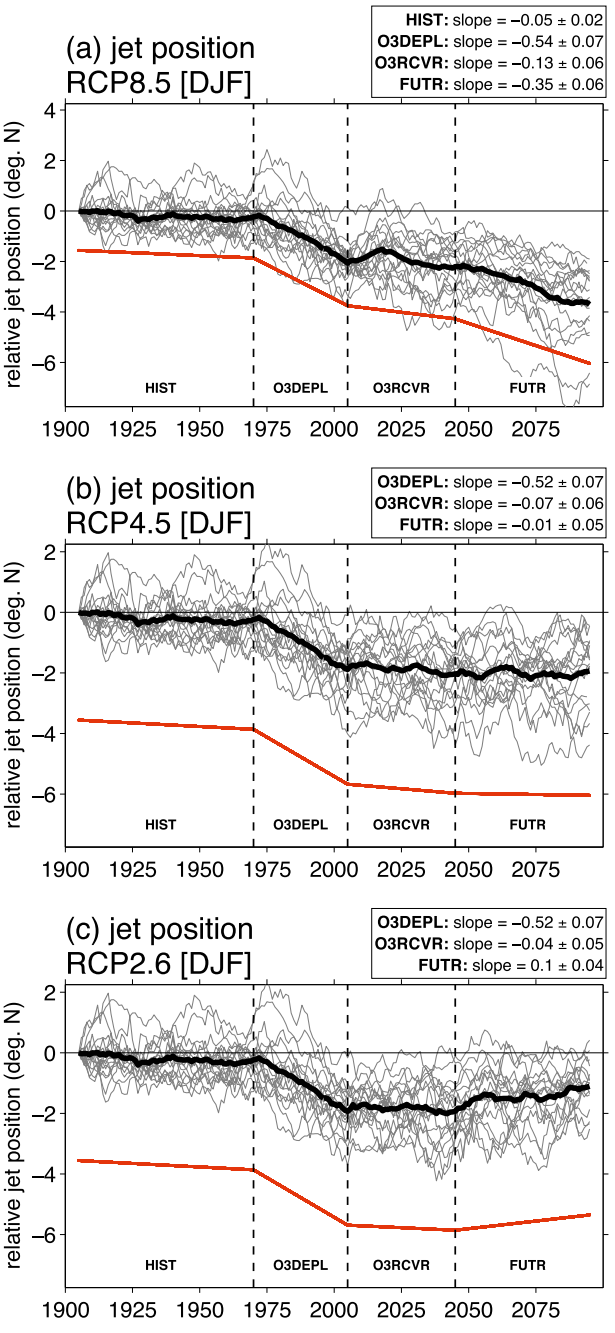

FIG. 1. Time series of the CMIP5 Southern Hemisphere DJF jet position relative to the 1900–10 value over the historical and three climate scenarios, (a) RCP8.5, (b) RCP4.5, and (c) RCP2.6. Thin black curves denote the individual models, and the multimodel mean is plotted in black. Red lines denote the piecewise linear least squares slopes, which are also given in the panels above in units of degrees per decade. Time series have been smoothed using a 10-yr moving average filter (see section 2d for details).

TABLE 3. Multimodel mean DJF shift (degrees north) of the midlatitude jet position. Negative values denote a poleward shift and positive values denote an equatorward shift. Year ranges below each period denote the edges of the period (beginning and end) used to calculate changes.

Period	Historical	RCP8.5	RCP4.5	RCP2.6
HIST, 1960–70 to 1900–10	−0.21°	—	—	—
O3DEPL, 2000–10 to 1960–70	—	−1.78°	−1.59°	−1.63°
O3RCVR, 2040–50 to 2000–10	—	−0.16°	−0.19°	−0.02°
FUTR, 2089–99 to 2040–50	—	−1.42°	+0.07°	+0.80°

influence of GHG emissions between 2005 and 2045 (Arblaster et al. 2011; Polvani et al. 2011a; McLandress et al. 2011). Similar conclusions are reached by Bracegirdle et al. (2013), who show that the RCP8.5 and RCP4.5 multimodel mean jet position exhibits reduced poleward trends between 2000 and 2049 compared to between 1960 and 1999 in the three Southern Hemisphere ocean basins.

The relative amount of cancellation between ozone recovery and GHGs can be seen by comparing the different RCPs during the O3RCVR period. The piecewise linear least squares slopes over each time period are plotted in red in Fig. 1, with the slopes given in units of degrees latitude per decade in the upper right-hand corner of each panel. The red lines are shifted from the thick black lines for clarity. RCP2.6 shows the smallest negative slope during O3RCVR ($-0.04°\,\text{decade}^{-1}$; which is not statistically different from zero) indicative of its smallest, but still increasing, GHG emissions. RCP4.5 exhibits a slightly negative trend ($-0.07°\,\text{decade}^{-1}$), and RCP8.5 exhibits a slightly more negative trend ($-0.13°\,\text{decade}^{-1}$), consistent with the larger emissions. Note that while RCP4.5 and RCP8.5 show the jet shifting poleward during O3RCVR, the negative slopes are significantly smaller than those seen during O3DEPL (approximately $-0.5°\,\text{decade}^{-1}$).

The varying amounts of cancellation of the poleward shift induced by GHGs among the different RCPs during O3RCVR confirm that GHGs are inducing a poleward trend in the circulation during the O3RCVR period; otherwise, the trends among the RCPs would be similar. The small magnitudes of the trends during O3RCVR compared to the O3DEPL and FUTR periods, however, suggest that the influence of GHGs is being opposed by ozone recovery during O3RCVR. This conclusion may appear to conflict with that of Chang et al. (2012), where they report no offset in the poleward migration of the DJF 250-hPa storm tracks over the first half to the twenty-first century under either RCP8.5 or RCP4.5. This difference, however, may be explained by the magnitude of the trends. The key message is that the projected trends will be smaller in 2005–45 than in 1960–2005: ozone recovery will delay the poleward migration of the summertime Southern Hemisphere jet over the next 30 years. After 2050, the importance of GHG emissions is evident, with RCP8.5 showing a continuation of the poleward shift, RCP4.5 showing no change in the jet position, and RCP2.6 showing the jet beginning to recover and return to its historical position as emissions are reduced.

The seasonal differences in the jet position trends provide further evidence that stratospheric ozone recovery is the forcing responsible for canceling the GHG-induced trends between 2005 and 2045. Figure 2 shows similar time series but for austral winter [June–August (JJA)], where the wintertime jet position shows no statistically significant trend before 2000 and then exhibits the same negative trend (approximately $-0.25°\,\text{decade}^{-1}$) over the entire twenty-first century in RCP8.5. The reduced trend projected in DJF over the O3RCVR period is absent in JJA. Note, however, GHGs and other forcings yield no JJA trends in the O3DEPL period: since these other forcings are likely not seasonal, this further suggests that the DJF trends in the models are largely due to ozone. This is additionally supported by the fact that the FUTR trend in JJA and DJF are not statistically different in either RCP8.5 (approximately $-0.3°\,\text{decade}^{-1}$) or RCP4.5 (approximately $0°\,\text{decade}^{-1}$), and to a lesser extent RCP2.6, highlighting that circulation trends not driven by ozone are similar throughout the two seasons. This further supports our conclusion that the reduced DJF trends between 2005 and 2045 are a result of stratospheric ozone recovery.

Vertical cross sections of the zonal wind changes provide evidence of a stratospheric polar influence; however, multimodel mean fields can skew the relative trends since some models exhibit large biases in the mean jet position. Because of this, in Fig. 3 we show the change in the DJF multimodel mean zonal-mean zonal winds, between the beginning and end of each period (difference between the edges of the period; see Table 3), as a function of relative latitude about the jet position at the start of the period. During O3DEPL (Figs. 3a–c), the positive zonal wind trends extend upward and poleward toward the region of stratospheric ozone depletion as was shown by Polvani et al. (2011b) using a model where only ozone varied. This leaves little doubt that the trends during this period are largely as a result of polar stratospheric ozone depletion. During the O3RCVR period (Figs. 3d–f), the trends are very weak and appear instead in the subtropical upper troposphere (approximately 30° north of the jet, or a latitude of 20°S), likely reflecting a response

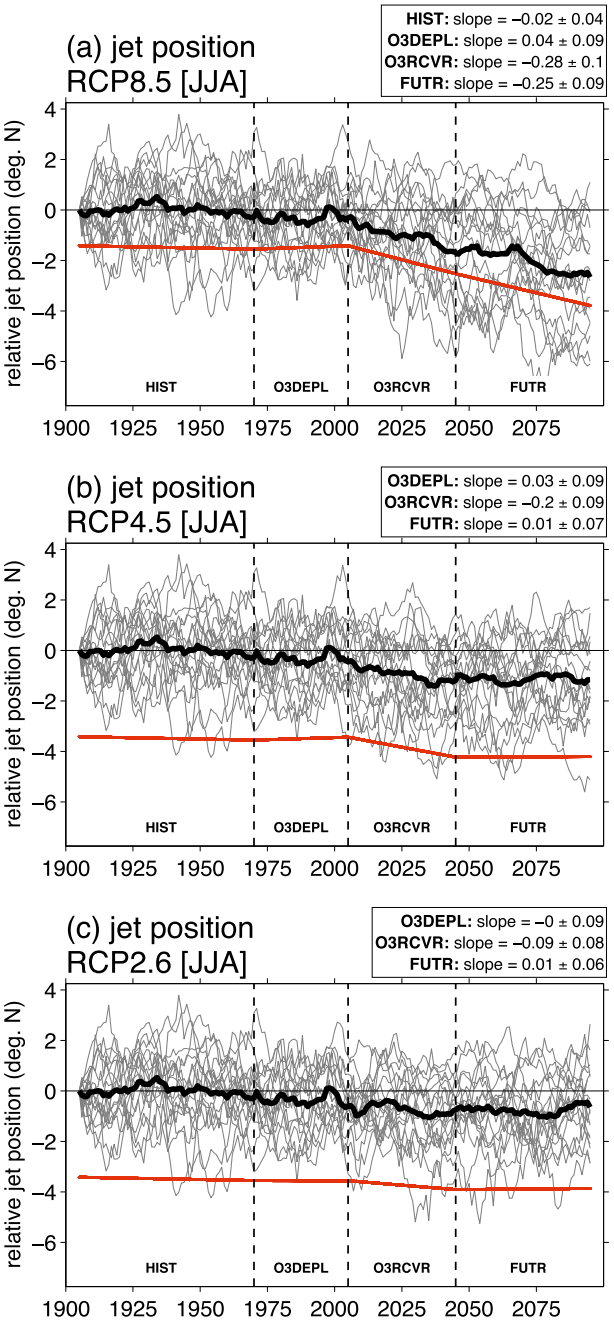

FIG. 2. As in Fig. 1, but for JJA.

to GHG-induced tropical warming (see, e.g., Polvani et al. 2011b). During the FUTR period (Fig. 3g), RCP8.5 exhibits trends indicating a poleward (southward) jet shift, although the tropospheric wind trends are weaker than they were during O3DEPL. In RCP4.5 (Fig. 3h), there is a small barotropic increase in the subtropical winds over the FUTR period, while RCP2.6 (Fig. 3i) exhibits a clear reversal of the midlatitude trends with the jet shifting equatorward. This result indicates that if GHG emissions are very aggressively reduced, the atmospheric circulation will begin to relax back to its pre–ozone hole position toward the end of this century.

4. Results from CMIP3

Further evidence that the reduced trends during the O3RCVR period are due to the cancellation of GHG-induced changes by ozone recovery is found in the CMIP3 model output. Some of the CMIP3 models did not include ozone depletion and recovery, while others did, and building on previous work (Son et al. 2008, 2009), we use these ozone differences to extract the signature of ozone depletion and recovery on future circulation trends by grouping the CMIP3 models into those with time-varying ozone (varyO3) and those without (fixO3).

Figure 4 shows the time series of jet position from the twentieth century and A1B experiments of the CMIP3 models. The trends for the varyO3 models (Fig. 4a) are most similar to those of the CMIP5 RCP8.5 simulations (Fig. 1a), with ozone depletion inducing a $-1.5°$ shift of the jet and ozone recovery canceling GHG-induced circulation trends, yielding an insignificant trend in the jet position between 2005 and 2045. The fixO3 models tell a different story (Fig. 4b), with the future trends in jet position across all three periods being statistically indistinguishable from one another at 95% confidence (calculated using a comparison of means).

The trends at the end of the twenty-first century (when ozone has recovered) in varyO3 and fixO3 are statistically the same (approximately $-0.2°\,\text{decade}^{-1}$), confirming that nonozone-forced circulation trends are similar across the two model groups. This supports our conclusion that differences between the trends during the O3DEPL and O3RCVR periods are due to the addition and cancellation of wind trends caused by ozone depletion and recovery. Furthermore, the jet position trends during O3DEPL are statistically the same between the CMIP3 varyO3 integrations and the CMIP5 RCP's (approximately $-0.5°\,\text{decade}^{-1}$), further strengthening the quantitative projections of the CMIP models.

5. Shifts in the subtropical dry zones

The cancellation of GHG-induced climate trends by ozone recovery is also found in another important measure of the atmospheric circulation: the extent of the subtropical dry zones. The expansion of the atmospheric overturning circulation (Hadley cell) and concurrent expansion of the subtropical dry zones has been documented in the observations (Seidel et al. 2008; Fu et al. 2006), and modeling studies suggest such a trend can be

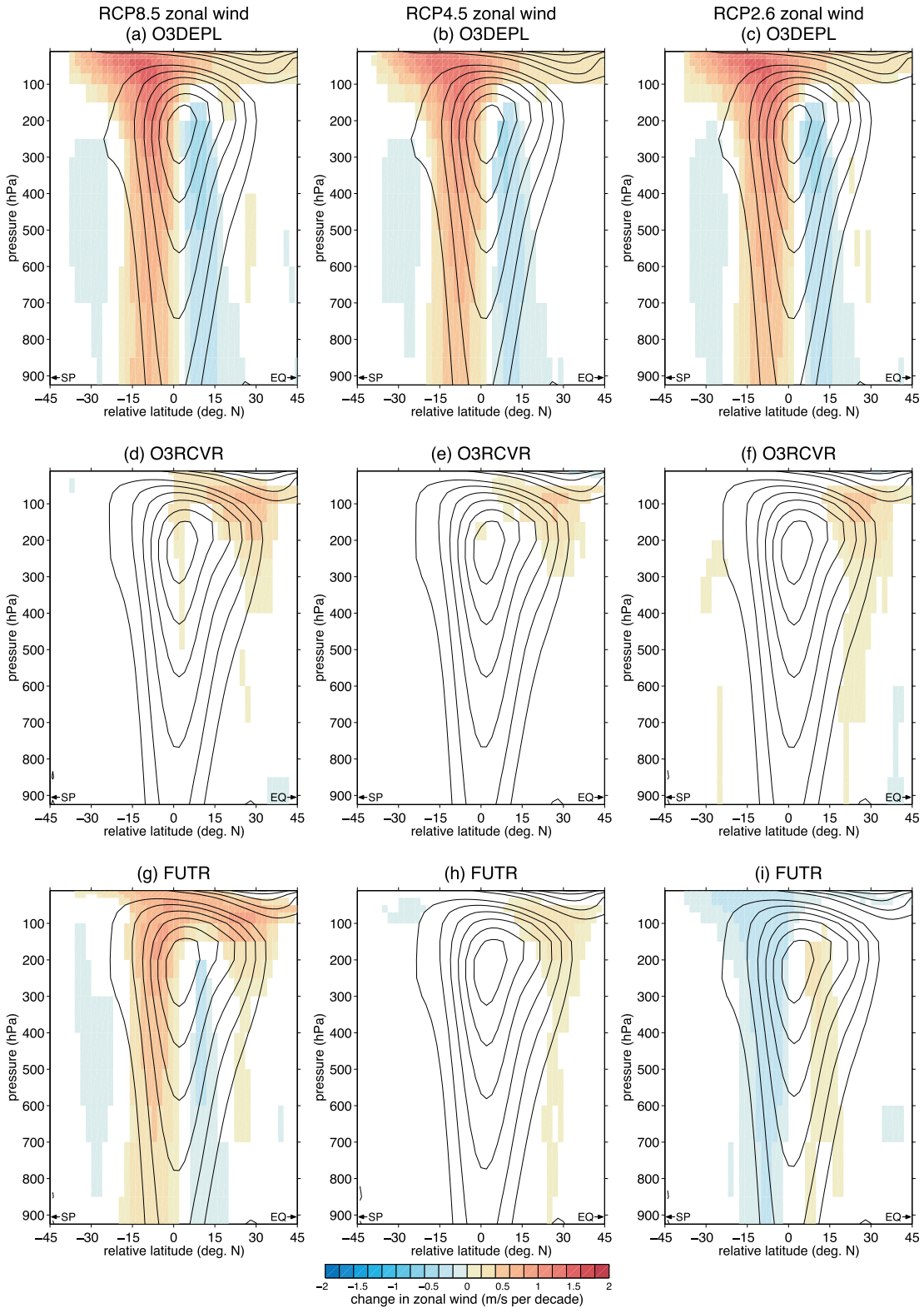

FIG. 3. Multimodel mean change ($m\,s^{-1}\,decade^{-1}$) of the DJF zonal-mean zonal winds for three climate scenarios grouped by period. The change is defined as the difference between the edges of the periods (see Table 3), and the black contours show the zonal-mean zonal wind fields for the earlier edge of each period. The plotting convention is such that the equator (EQ) is to the right and the South Pole (SP) is to the left in each panel. Fields were interpolated to a 2° by 2° lat–lon grid before plotting.

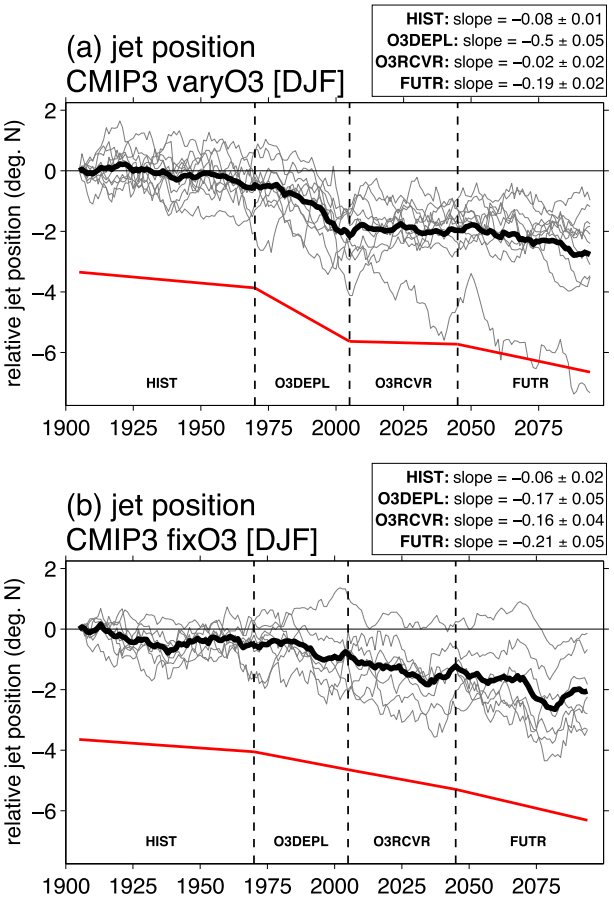

FIG. 4. As in Fig. 1, but for the CMIP3 models, separated by those models (a) with time-varying stratospheric ozone and those (b) with fixed ozone.

induced by increasing GHG emissions and/or stratospheric ozone depletion (Lu et al. 2009; Polvani et al. 2011b; McLandress et al. 2011). Scheff and Frierson (2012a) show that the CMIP5 models robustly exhibit a poleward expansion of the subtropical dry zones between the end of the twentieth and twenty-first centuries, and we extend their analysis by looking year by year at the trends in the DJF dry zone edge.

As seen in Fig. 5, the largest trends in the subtropical dry zone extent occur during the O3DEPL and FUTR periods. Statistically insignificant trends are present during O3RCVR, when ozone recovery largely cancels the effects of GHG emission increases. The dry zones continue to expand in RCP8.5 during the FUTR period (Fig. 5a), level off in RCP4.5 (Fig. 5b), and rebound toward their historical positions in RCP2.6 (Fig. 5c). Trends in the dry zone edge for JJA (not shown) give similar poleward slopes in both the O3DEPL and O3RCVR periods, confirming that differences in the trends over these two periods are confined to DJF.

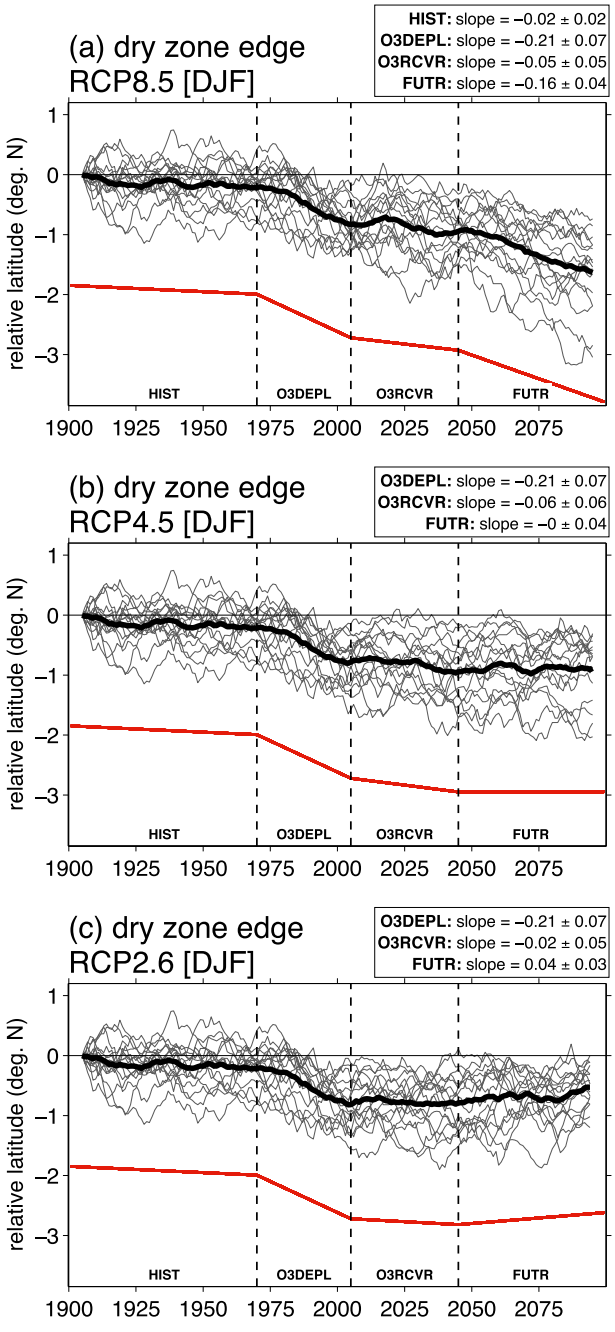

FIG. 5. As in Fig. 1, but for the latitude of the subtropical dry zone edge (precipitation minus evaporation zero crossing).

We wish to emphasize that while the midlatitude jet position is computed using the lower-tropospheric zonal-mean zonal winds, the dry zone edge is computed using the moisture fluxes, namely, where the zonal-mean precipitation minus evaporation is zero (see section 2). Thus, the strong similarities between the jet trends and dry zone edge trends between 1900 and 2100 (Figs. 1 and 5) are not because we are using similar model

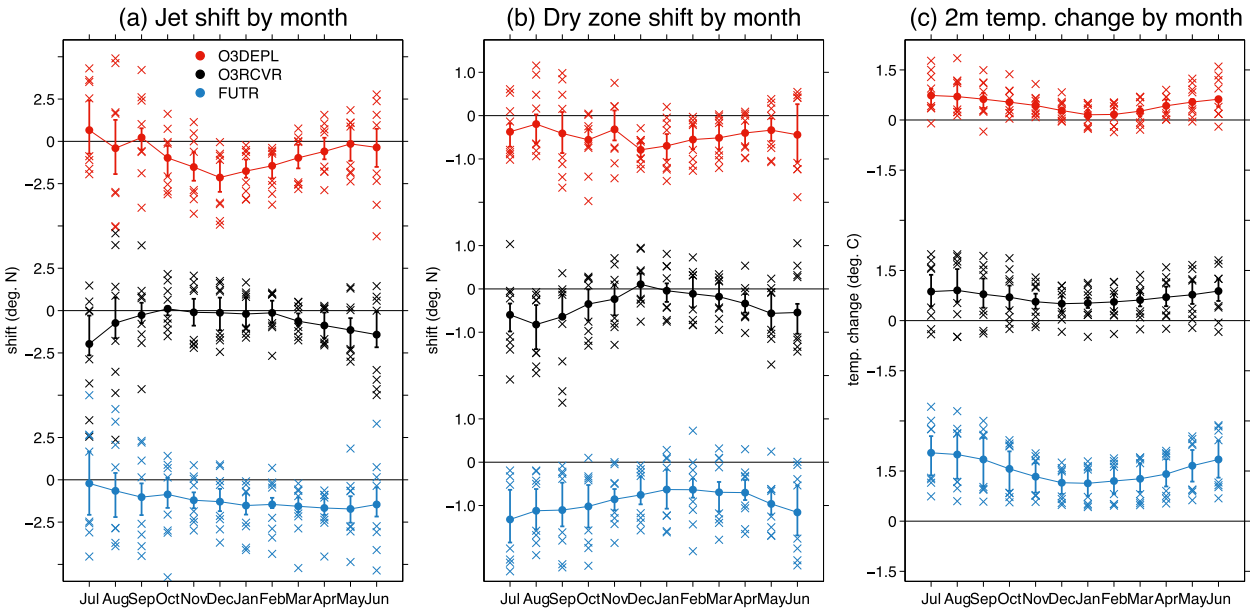

FIG. 6. Shift in the Southern Hemisphere (a) jet and (b) dry zone edge (zero crossing of precipitation minus evaporation) as a function of month for three time periods over the historical and RCP8.5 scenarios. (c) Similar to (a),(b), but for the area-averaged high-latitude (46°–90°S) 2-m air temperature. In all panels, the bars denote the 25th–75th percentile range, and the crosses denote values outside of this interval. The calculation is done as a time-slice difference, and the years used for each time period are given in Table 3.

diagnostics: rather, they confirm a broad hemispheric-wide response of the circulation to stratospheric ozone depletion and recovery. These similarities also support the conclusions of Scheff and Frierson (2012b), whereby the shifts in the hydrological cycle are coupled to the simultaneous poleward shift of the Hadley cell edge with the midlatitude storm tracks and jet.

6. Seasonality of the circulation trends

The seasonality of stratospheric ozone depletion and recovery is documented extensively in the model-based literature (see, e.g., Eyring et al. 2013). We exploit this seasonality to provide further evidence that the reduced trends in the period 2005–45 are largely a result of stratospheric ozone recovery canceling the effects of GHG increases. Figure 6a shows the total shift in the jet latitude as a function of month and time period for RCP8.5; similarly, Fig. 6b shows the shift in the subtropical dry zone edge. During the O3DEPL period (1970–2005; red curves), the largest poleward shifts are found in the summer, when springtime stratospheric ozone depletion induces the largest tropospheric response; no consistent trend among the models is found during the winter months, as previously shown. During the O3RCVR period (2005–45; black curves), most models exhibit a poleward shift of the jet and dry zone edge outside of the summer months. The near-zero multimodel mean shift during summer confirms that ozone recovery is canceling the GHG-induced shift in DJF. When ozone has largely recovered (2045–2100; blue curves), there is less seasonal variation in the trends of the jet and subtropical dry zone positions. This further supports the conclusion that the seasonality of the trends during the O3DEPL period cannot be due to GHGs alone, as these influence the circulation year-round. Note that the seasonality of trends in Fig. 6a is clearer than Fig. 6b, since the ozone signal weakens with distance from the pole as noted by Polvani et al. (2011b).

7. Seasonal surface temperature trends

Bitz and Polvani (2012) studied the effects of stratospheric ozone depletion on Southern Hemisphere surface temperatures using an ocean eddy–resolving coupled climate model and found that the annual-mean mid- to high-latitude surface temperatures warmed with ozone depletion. The opposite response is expected to follow from the projected recovery of stratospheric ozone, as suggested by the results of Smith et al. (2012). In this section we investigate whether a surface temperature response to ozone depletion and recovery can be identified in the Southern Hemisphere climate in CMIP5.

The RCP8.5 simulations show a monotonic increase of 2-m air temperature over the Southern Ocean (46°–90°S) in the annual mean (Fig. 7a), with the warming trends increasing steadily with time over the next century. The summer and winter months, individually, also

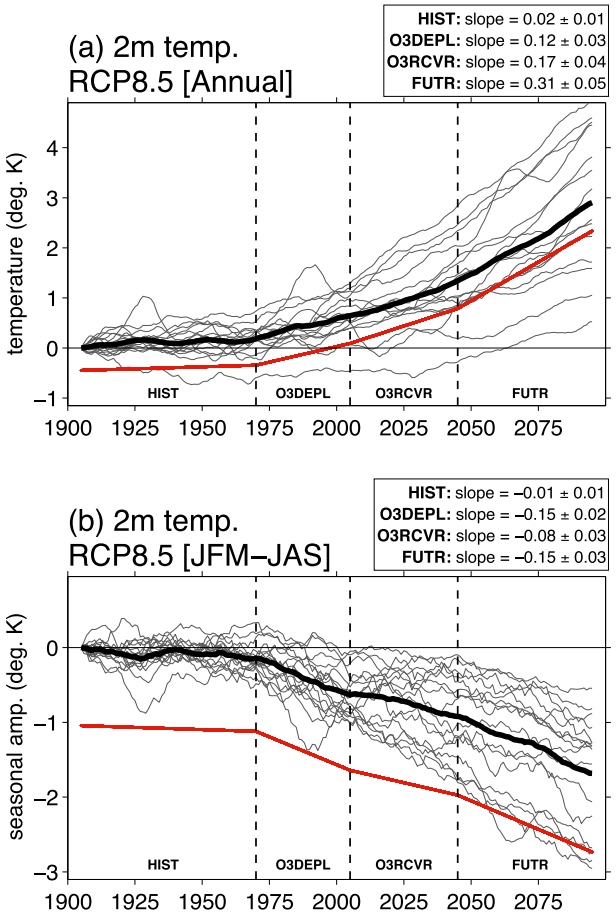

FIG. 7. As in Fig. 1, but for the RCP8.5 high-latitude (46°–90°S) 2-m air temperature for the (a) annual mean and (b) seasonal amplitude defined as summer minus winter (JFM − JAS).

show increasing temperature trends over the next century (not shown). Since the warming over the twenty-first century does not appear to slow down during O3RCVR, we are unable to extract the ozone signal from near-surface temperatures directly.

A surface temperature signal from stratospheric ozone recovery is apparent, however, when the seasonal cycle of the trends is considered. Figure 6c shows the monthly change in mid- to high-latitude (46°–90°S) 2-m air temperatures. The overall positive trends in Fig. 6c indicate that the 2-m air temperatures are warming throughout the year. However, note that during O3DEPL (red curve), the winter months [July–September (JAS)] warm more than the summer months [January–March (JFM)]. This preference for warming during the winter relative to summer is also evident over the FUTR period. In contrast, only a weak seasonal signal is present over the O3RCVR period.

This seasonal cycle of the warming can be exploited to extract the surface warming signal in O3DEPL relative to O3RCVR. We define the "seasonal amplitude" of the 2-m air temperature as the difference between the mean summertime (JFM) and wintertime (JAS) temperatures. This quantity is always positive, since the summer is on the order of 7°C warmer than the winter in the models. Note that the seasonal temperature response in Fig. 6c is lagged by 1 month (smallest O3DEPL trends in January) compared to the jet and dry zone edge responses (Figs. 6a,b; smallest O3DEPL trends in December), supporting the use of JFM and JAS, rather than DJF and JJA as done in the previous sections.

Figure 7b shows the changes in the seasonal amplitude of 2-m air temperature in RCP8.5: these changes exhibit similar signatures of ozone depletion and recovery as previously discussed for other quantities (Figs. 1 and 5). Negative trends imply that the winter is warming more than the summer (the difference between the winter and summer temperatures is decreasing) and the winter warms more than the summer in all three future periods. However, the O3RCVR exhibits smaller negative trends in seasonal amplitude compared to the O3DEPL and FUTR periods, providing evidence that ozone depletion may have induced a greater warming of winter relative to summer over the O3DEPL period and that ozone recovery may mitigate future winter warming relative to the summer.

To mechanistically understand the role of ozone depletion and recovery on the trends in the seasonal amplitude of 2-m temperature, we show latitude–longitude plots of its multimodel mean change (end of period minus beginning of period) in Fig. 8 for the three RCPs. Looking first at O3DEPL (Figs. 8a–c), an annular pattern emerges, with a decrease in the seasonal amplitude (blue shading; warming of the winter relative to the summer) confined poleward of 46°S (solid black line) and an increase in the seasonal amplitude (yellow and red shading; cooling of winter relative to the summer) equatorward of 46°S. While we are unaware of previous studies explicitly showing the accelerated surface warming of the winter relative to summer induced by ozone depletion, or the effects of ozone recovery on the seasonal warming signal, the mechanism behind the seasonal response of surface temperature from stratospheric ozone depletion has been previously suggested (Sigmond and Fyfe 2010; Bitz and Polvani 2012; Smith et al. 2012); we briefly summarize it here.

During the O3DEPL period, stratospheric cooling in the springtime from ozone loss induces a poleward shift of the midlatitude winds during summer. The shift of the summertime near-surface winds both warms the ocean surface by mixing warmer waters up from below and by inducing an anomalous meridional overturning circulation that transports cold high-latitude surface water

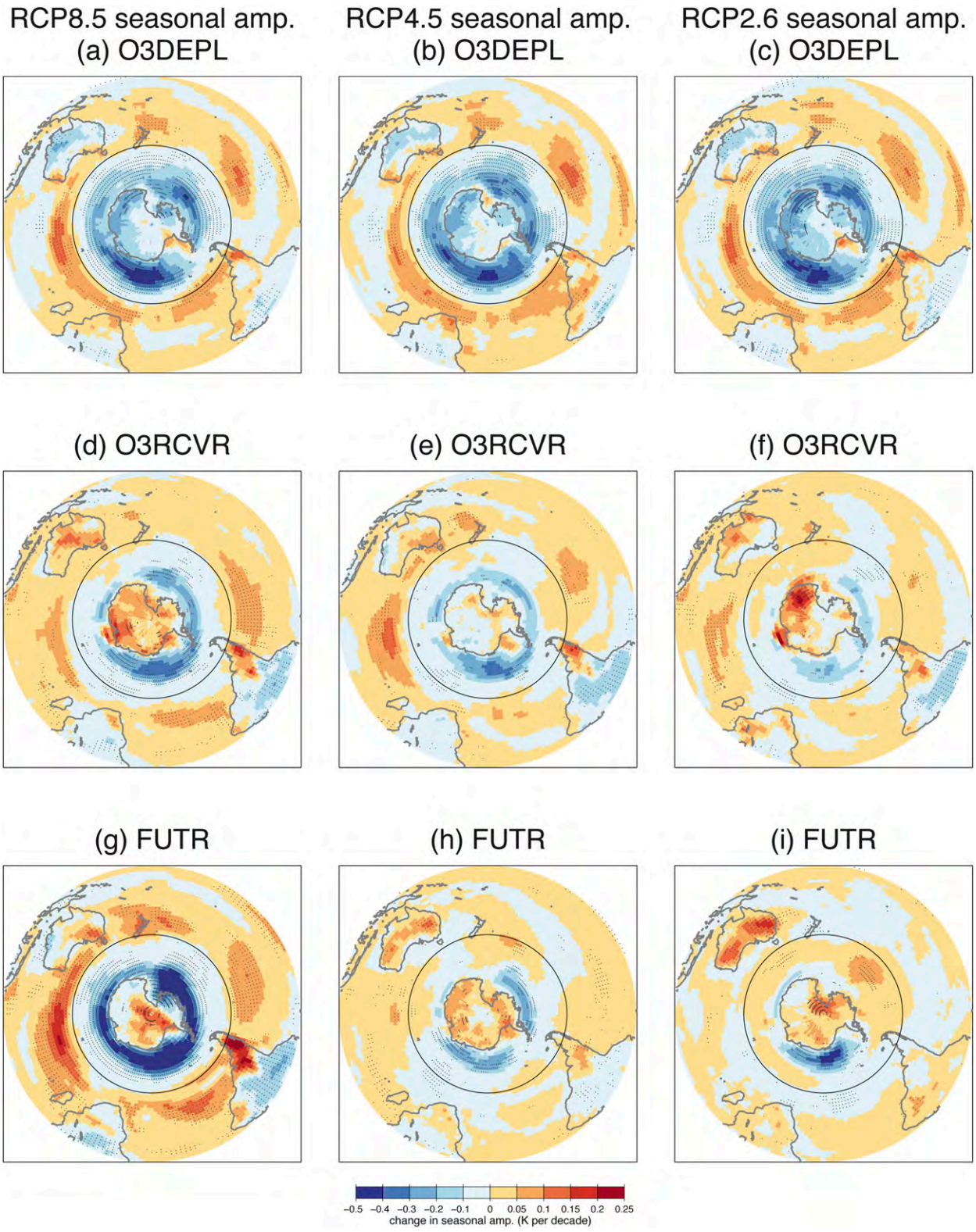

FIG. 8. Multimodel mean change in degrees per decade of the seasonal amplitude of 2-m air temperatures. Stippling denotes locations where at least 80% of the models (13 of 16) agree on the sign of the change. Solid black lines denote the multimodel mean jet position at the beginning of the O3DEPL period (46°S; see Table 3 for the years included in each period). Fields were interpolated to a 2° by 2° lat–lon grid before plotting.

equatorward and warm low-latitude surface water poleward. Thus, in summer during O3DEPL, the ocean surface is warmer equatorward of the jet compared to poleward of the jet. In winter during O3DEPL, although the wind anomalies are no longer present, the ocean surface remains anomalously warm because of the long oceanic time scales. In addition to the ocean anomalies themselves, a warmer ocean surface leads to basal melting and a reduction in sea ice growth, which allows for increased surface absorption of shortwave fluxes in summer. This anomalous energy input into the ocean is released to the atmosphere during winter when the air–sea temperature difference is maximized, further increasing the high-latitude winter air temperatures relative to summer (Manabe and Stouffer 1980; Manabe et al. 1992; Bitz and Polvani 2012; Dwyer et al. 2012). Putting all of this together, the high-latitude warming in winter is larger than in summer, and the low-latitude warming in winter is smaller than in summer, creating a dipolar pattern of the seasonal amplitude trends during the O3DEPL period (Figs. 8a–c).

This mechanism suggests that during the ozone depletion period, anomalous surface air temperatures are driven by anomalous ocean temperatures that, in turn, are driven by shifts in the atmospheric circulation. In support of the role of the atmospheric circulation driving the air temperature trends, we overlay the 1960–70 multimodel mean jet latitude (46°S) as a black line in all panels of Fig. 8; the seasonal amplitude trend pattern aligns well with the latitude of the jet during O3DEPL. In addition, as ozone recovers between 2005 and 2045, the jet shift is reduced in all RCPs (Fig. 1), and one might expect this to reduce the trends in the seasonal amplitude during O3RCVR. Indeed, trends during O3RCVR shown in Figs. 8d–f are weaker, and there is less model agreement than during O3DEPL. In addition, RCP2.6 exhibits the smallest circulation trends during the O3RCVR period (Figs. 1, 5) and also exhibits the smallest change in seasonal amplitude among the RCPs during this period (Fig. 8f).

We conclude this section by discussing the FUTR period, when stratospheric ozone has largely recovered. The patterns of the trends in 2-m air temperature for the FUTR period are shown in Figs. 8g–i. For RCP4.5, the circulation response is weak in the FUTR period and similarly so are the changes in the seasonal amplitude. For RCP2.6, although model agreement is low, the sign of the changes in seasonal amplitude have reversed during the FUTR period compared to the O3DEPL period in most locations except for east of the Weddell Sea. This is consistent with the circulation beginning to recover during this period. Finally, for RCP8.5, the trend patterns and magnitudes appear similar to those during O3DEPL (Fig. 8a). However, during the FUTR period, the response of the seasonal amplitude cannot be easily explained by the ocean circulation and mixing mechanism described above, since the GHG-induced wind anomalies occur year-round (Fig. 6a; blue line) and the mechanism requires that the wind anomalies occur in the summer only (as is the case for ozone depletion). We do not know why the trend pattern over the FUTR period is so similar to that over the O3DEPL, but previous studies suggest that the high-latitude accelerated warming of winter relative to summer with increased GHG concentrations can be explained by the changes in air–sea fluxes associated with sea ice loss (Manabe and Stouffer 1980; Manabe et al. 1992; Dwyer et al. 2012). It is also possible that seasonal differences in the wind strength response could cause the seasonal amplitude patterns in Figs. 8g–i; however, determining what drives the midlatitude increase in the seasonal amplitude between 2045 and 2100 is beyond the scope of this study.

8. Antarctic sea ice trends

As described in the previous section, ozone depletion warms the ocean surface through changes in the tropospheric winds, and this ocean warming limits sea ice growth. The response of sea ice concentrations to ozone depletion and recovery can be seen in the time series of the JFM sea ice area (Fig. 9) in RCP8.5. The largest decrease in sea ice area occurs during the O3DEPL period, when high-latitude warming both melts the sea ice and the anomalous surface wind stress (from the jet shift) transports the ice away from the continent (Sigmond and Fyfe 2010; Bitz and Polvani 2012). This modeled Antarctic sea ice decrease in the last three decades is at odds with observations, which show a small yet statistically significant increase in sea ice extent (Liu et al. 2004; Holland and Kwok 2012; Turner et al. 2013). The difference remains unexplained; however, a recent study by Polvani and Smith (2013) suggests that this discrepancy may be explained by internal variability since the observed trends fall within the bounds of the natural variability of the system.

Contrasting the JFM and JAS panels in Fig. 9, one can see that the relative changes in sea ice area, in O3DEPL, are much stronger in JFM than in JAS, in agreement with Sigmond and Fyfe (2010). In the coming decades, however, the CMIP5 models project that ozone recovery will mitigate the effects of increasing GHGs on summer Antarctic sea ice. This can be seen from the fact that the rate of JFM sea ice loss over the O3RCVR period is nearly half of that during O3DEPL, in agreement with Smith et al. (2012).

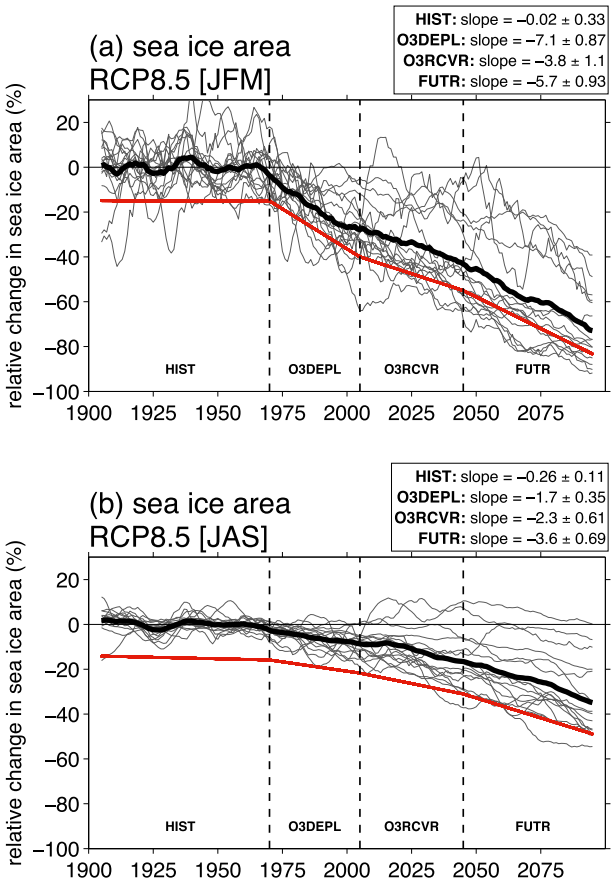

FIG. 9. As in Fig. 1, but for the RCP8.5 (a) JFM and (b) JAS percent change in sea ice area.

9. Conclusions

We have demonstrated, using transient climate simulations from 18 CMIP5 models, that stratospheric ozone recovery will be a major driver of Southern Hemisphere climate over the twenty-first century. Focusing on specific time periods based on the trends in stratospheric ozone forcing and exploiting the seasonality of ozone depletion and recovery to separate the ozone signal from that of other climate forcings, we have shown that the CMIP5 models clearly project delayed climate change over the entire Southern Hemisphere in summer as a consequence of ozone recovery. This reduced climate change manifests itself in the summertime Southern Hemisphere winds, dry zone edge, surface temperatures, and Antarctic sea ice concentrations. To further elucidate the contribution of stratospheric ozone depletion and recovery on the summertime tropospheric trends over the twenty-first century, we compare results from three different forcing scenarios (RCPs 8.5, 4.5, and 2.6) and demonstrate the respective cancellation between the trends driven by stratospheric ozone and those driven by increasing GHG emissions across a range of climate scenarios.

These results highlight the perhaps surprising fact that the changes in the simulated summertime tropospheric circulation between 1970 and 2005, driven largely by stratospheric ozone depletion, are of comparable magnitude (or larger) than the projected changes in *any* scenario over the entire twenty-first century (see Table 3). Previous studies based on targeted model experiments using a single model (Arblaster and Meehl 2006; Polvani et al. 2011a; McLandress et al. 2011) have suggested ozone recovery would cancel a significant portion of the GHG-induced changes between 2000 and 2045. Our study supports this conclusion, showing that the transient future simulations from 18 CMIP5 models exhibit delayed Southern Hemisphere climate change as a consequence of ozone recovery. In addition, the CMIP5 future ''best-case'' emissions scenario (RCP2.6), where GHG emissions decrease throughout the late twenty-first century, demonstrates that by 2100 the circulation rebounds only 40% of the distance caused by twentieth-century ozone depletion (Fig. 1c). Finally, while the most robust response to future climate change is a warming over Earth's surface, our results suggest that ozone recovery may modify the seasonal fingerprint of the temperature signal over the first half of the twenty-first century.

Acknowledgments. We acknowledge Haibo Liu for obtaining the CMIP5 data, Darryn Waugh for helpful discussions, and three anonymous reviewers for their helpful comments. We acknowledge the World Climate Research Programme's Working Group on Coupled Modelling, which is responsible for CMIP, and we thank the climate modeling groups for producing and making available their model output. For CMIP the U.S. Department of Energy's Program for Climate Model Diagnosis and Intercomparison provides coordinating support and led development of software infrastructure in partnership with the Global Organization for Earth System Science Portals. EAB is funded by a NOAA Climate and Global Change Fellowship through the University Corporation of Atmospheric Research Visiting Science Program. LMP is funded, in part, by a grant of the U.S. National Science Foundation to Columbia University.

REFERENCES

Arblaster, J. M., and G. A. Meehl, 2006: Contributions of external forcings to southern annular mode trends. *J. Climate,* **19,** 2896–2905.

——, ——, and D. J. Karoly, 2011: Future climate change in the Southern Hemisphere: Competing effects of ozone and greenhouse gases. *Geophys. Res. Lett.,* **38,** L02701, doi:10.1029/2010GL045384.

Barnes, E. A., and L. M. Polvani, 2013: Response of the midlatitude jets, and of their variability, to increased greenhouse gases in the CMIP5 models. *J. Climate,* **26,** 7117–7135.

Bitz, C. M., and L. M. Polvani, 2012: Antarctic climate response to stratospheric ozone depletion in a fine resolution ocean climate model. *Geophys. Res. Lett.,* **39,** L20705, doi:10.1029/2012GL053393.

Bracegirdle, T. J., E. Shuckburgh, J.-B. Sallee, Z. Wang, A. J. S. Meijers, N. Bruneau, T. Phillips, and L. J. Wilcox, 2013: Assessment of surface winds over the Atlantic, Indian, and Pacific Ocean sectors of the Southern Ocean in CMIP5 models: Historical bias, forcing response, and state dependence. *J. Geophys. Res.,* **118,** 547–562, doi:10.1002/jgrd.50153.

Ceppi, P., Y. Hwang, D. Frierson, and D. Hartmann, 2012: Southern Hemisphere jet latitude biases in CMIP5 models linked to shortwave cloud forcing. *Geophys. Res. Lett.,* **39,** L19708, doi:10.1029/2012GL053115.

Chang, E. K. M., Y. Guo, and X. Xia, 2012: CMIP5 multimodel ensemble projection of storm track change under global warming. *J. Geophys. Res.,* **117,** D23118, doi:10.1029/2012JD018578.

Cionni, I., and Coauthors, 2011: Ozone database in support of CMIP5 simulations: Results and corresponding radiative forcing. *Atmos. Chem. Phys.,* **11,** 11 267–11 292, doi:10.5194/acp-11-11267-2011.

Cordero, E. C., and P. M. F. Forster, 2006: Stratospheric variability and trends in models used for the IPCC AR4. *Atmos. Chem. Phys.,* **6,** 5369–5380.

Dwyer, J. G., M. Biasutti, and A. H. Sobel, 2012: Projected changes in the seasonal cycle of surface temperature. *J. Climate,* **25,** 6359–6374.

Eyring, V., and Coauthors, 2013: Long-term ozone changes and associated climate impacts in CMIP5 simulations. *J. Geophys. Res.,* **118,** 5029–5060, doi:10.1002/jgrd.50316.

Fu, Q., C. Johanson, J. Wallace, and T. Reichler, 2006: Enhanced mid-latitude tropospheric warming in satellite measurements. *Science,* **312,** 1179, doi:10.1126/science.1125566.

Holland, P. R., and R. Kwok, 2012: Wind-driven trends in Antarctic sea-ice drift. *Nat. Geosci.,* **5,** 872–875, doi:10.1038/NGEO1627.

Kang, S. M., L. M. Polvani, J. C. Fyfe, and M. Sigmond, 2011: Impact of polar ozone depletion on subtropical precipitation. *Science,* **332,** 951–954.

Kidston, J., and E. Gerber, 2010: Intermodel variability of the poleward shift of the austral jet stream in the CMIP3 integrations linked to biases in the 20th century climatology. *Geophys. Res. Lett.,* **37,** L09708, doi:10.1029/2010GL042873.

Lee, S., and S. B. Feldstein, 2013: Detecting ozone- and greenhouse gas–driven wind trends with observational data. *Science,* **339,** 563–567, doi:10.1126/science.1225154.

Liu, J., J. Curry, and D. Martinson, 2004: Interpretation of recent Antarctic sea ice variability. *Geophys. Res. Lett.,* **31,** L02205, doi:10.1029/2003GL018732.

Lu, J., C. Deser, and T. Reichler, 2009: Cause of the widening of the tropical belt since 1958. *Geophys. Res. Lett.,* **36,** L03803, doi:10.1029/2008GL036076.

Manabe, S., and R. Stouffer, 1980: Sensitivity of a global climate model to an increase of CO_2 concentration in the atmosphere. *J. Geophys. Res.,* **85** (80), 5529–5554.

——, M. Spelman, and R. Stouffer, 1992: Transient responses of a coupled ocean–atmosphere model to gradual changes of atmospheric CO_2. Part II: Seasonal response. *J. Climate,* **5,** 105–126.

McLandress, C., T. G. Shepherd, J. F. Scinocca, D. A. Plummer, M. Sigmond, A. I. Jonsson, and M. C. Reader, 2011: Separating the dynamical effects of climate change and ozone depletion. Part II: Southern Hemisphere troposphere. *J. Climate,* **24,** 1850–1868.

Meehl, G. A., C. Covey, T. Delworth, M. Latif, B. McAvaney, J. F. B. Mitchell, R. J. Stouffer, and K. E. Taylor, 2007: The WRCP CMIP3 multimodel dataset: A new era in climate change research. *Bull. Amer. Meteor. Soc.,* **88,** 1383–1394.

Meinshausen, M., and Coauthors, 2011: The RCP greenhouse gas concentrations and their extensions from 1765 to 2300. *Climatic Change,* **109,** 213–241, doi:10.1007/s10584-011-0156-z.

Polvani, L. M., and S. Solomon, 2012: The signature of ozone depletion on tropical temperature trends, as revealed by their seasonal cycle in model integrations with single forcings. *J. Geophys. Res.,* **117,** D17102, doi:10.1029/2012JD017719.

——, and K. L. Smith, 2013: Can natural variability explain observed Antarctic sea ice trends? New modeling evidence from CMIP5. *Geophys. Res. Lett.,* **40,** 3195–3199, doi:10.1002/grl.50578.

——, M. Previdi, and C. Deser, 2011a: Large cancellation, due to ozone recovery, of future Southern Hemisphere atmospheric circulation trends. *Geophys. Res. Lett.,* **38,** L04707, doi:10.1029/2011GL046712.

——, D. Waugh, G. Correa, and S. Son, 2011b: Stratospheric ozone depletion: The main driver of twentieth-century atmospheric circulation changes in the Southern Hemisphere. *J. Climate,* **24,** 795–812.

Roscoe, H., and J. Haigh, 2007: Influences of ozone depletion, the solar cycle and the QBO on the southern annular mode. *Quart. J. Roy. Meteor. Soc.,* **133,** 1855–1864, doi:10.1002/qj.153.

Scheff, J., and D. Frierson, 2012a: Robust future precipitation declines in CMIP5 largely reflect the poleward expansion of model subtropical dry zones. *Geophys. Res. Lett.,* **39,** L18704, doi:10.1029/2012GL052910.

——, and ——, 2012b: Twenty-first-century multimodel subtropical precipitation declines are mostly midlatitude shifts. *J. Climate,* **25,** 4330–4347.

Seidel, D. J., Q. Fu, W. J. Randel, and T. J. Reichler, 2008: Widening of the tropical belt in a changing climate. *Nat. Geosci.,* **1,** 21–24.

Sigmond, M., and J. C. Fyfe, 2010: Has the ozone hole contributed to increased Antarctic sea ice extent? *Geophys. Res. Lett.,* **37,** L18502, doi:10.1029/2010GL044301.

Smith, K. L., L. M. Polvani, and D. R. Marsh, 2012: Mitigation of 21st century Antarctic sea ice loss by stratospheric ozone recovery. *Geophys. Res. Lett.,* **39,** L20701, doi:10.1029/2012GL053325.

Son, S. W., L. Polvani, D. Waugh, and H. Akiyoshi, 2008: The impact of stratospheric ozone recovery on the Southern Hemisphere westerly jet. *Science,* **320,** 1486–1489, doi:10.1126/science.1155939.

——, N. F. Tandon, L. M. Polvani, and D. W. Waugh, 2009: Ozone hole and Southern Hemisphere climate change. *Geophys. Res. Lett.,* **36,** L15705, doi:10.1029/2009GL038671.

——, and Coauthors, 2010: The impact of stratospheric ozone on the Southern Hemisphere circulation changes: A multimodel assessment. *J. Geophys. Res.,* **115,** D00M07, doi:10.1029/2010JD014271.

Thompson, D. W. J., and S. Solomon, 2002: Interpretation of recent Southern Hemisphere climate change. *Science,* **296,** 895–899.

——, ——, P. J. Kushner, M. H. England, K. M. Grise, and D. J. Karoly, 2011: Signatures of the Antarctic ozone hole in Southern Hemisphere surface climate change. *Nat. Geosci.,* **4,** 741–749, doi:10.1038/ngeo1296.

Turner, J., T. J. Bracegirdle, T. Phillips, G. J. Marshall, and J. S. Hosking, 2013: An initial assessment of Antarctic sea ice extent in the CMIP5 models. *J. Climate,* **26,** 1473–1484.

Waugh, D. W., F. Primeau, T. Devries, and M. Holzer, 2013: Recent changes in the ventilation of the southern oceans. *Science,* **339,** 568–570, doi:10.1126/science.1225411.

Wilcox, L. J., A. J. Charlton-Perez, and L. J. Gray, 2012: Trends in austral jet position in ensembles of high- and low-top CMIP5 models. *J. Geophys. Res.,* **117,** D13115, doi:10.1029/2012JD017597.

Wu, Y., R. Seager, M. Ting, N. Naik, and T. Shaw, 2012: Atmospheric circulation response to an instantaneous doubling of carbon dioxide. Part I: Model experiments and transient thermal response in the troposphere. *J. Climate,* **25,** 2862–2879.